Journal of Electroanalytical Chemistry 782 (2016) 182–191

Contents lists available at ScienceDirect

Journal of Electroanalytical Chemistry

journal homepage: www.elsevier.com/locate/jelechem

Electrochemical synthesis and characterization of self-supported polypyrrole-DBS-MWCNT electrodes

Toribio F. Otero [a], Johanna Schumacher [b,*]

[a] Laboratory of Electrochemistry and Intelligent Materials, Technical University of Cartagena, ETSII, Campus Alfonso XIII, 30203 Cartagena, Spain
[b] Arquimea Ingeniería, Margarita Salas 10, 28919 Leganés, Spain

ARTICLE INFO

Article history:
Received 27 June 2016
Received in revised form 7 October 2016
Accepted 10 October 2016
Available online 11 October 2016

Keywords:
Polypyrrole composites
Self-supported electrodes
Carbon nanotubes
Reaction-driven conformations
Cation-exchanges

ABSTRACT

The electrochemical conditions (electrolyte potential window, monomeric oxidation) for the synthesis of polypyrrole-dodecylbenzenesulfonate-multiwalled carbon nanotube (PPy-DBS-MWCNT) composite were determined. Thick PPy-DBS-MWNT films were electrogenerated and peeled off from the working electrode. Self-supported PPy-DBS-MWCNT electrodes were fabricated. The morphology of the film was analyzed by SEM. Self-supported electrodes were characterized by potential cycling and by consecutive square potential waves in $NaClO_4$ aqueous solution with different cathodic potential limits. Higher reduced structures (the current never drops to zero) are obtained and analyzed from voltammetric responses until rising cathodic potential limits (up to −5 V). For high cathodic potentials (>−1 V) a slow hydrogen evolution coexists with the film reduction, as revealed from coulovoltammetric (charge-potential) responses, and the reduction rate decreases without significant polymeric degradation. Degradation of the material electroactivity in $NaClO_4$ is initiated by anodic overpotentials beyond 1.2 V. Both, oxidation and reduction chronoamperometric responses prove the presence of nucleation processes, most significant during oxidation. Chronocoulometric responses illustrate slower oxidation rates from deeper reduced initial states. The electrochemical responses are explained by reaction-driven conformational and structural changes that are clarified by the coulovoltammetric responses.

1. Introduction

Electroactive films based on conducting polymers (CP) are oxidized and reduced in electrolytes under electrochemical control. During the redox reaction charges are generated on the electroactive polymeric centers, counterions are exchanged with the electrolyte for charge balance in the film and solvent, for osmotic balance [1–3]. The reaction drives the variation of the polymeric charge and ionic concentration inside the film, which is causative for the reversible value change of a wide range of properties (e.g. volume, conductivity, color, stored charge) [4–6]. Those responsive properties motivate the synthesis and characterization of novel materials based on CPs in view of the development of new electrochemical devices [7]. Numerous electrochemical studies have been conducted for different materials based on CPs such as basic CPs [8–10], CP blends [11–15] and carbon based CP composites like conducting polymer-carbon nanotubes (CP-CNT) composites [16–18].

CP-CNT composites can be prepared by chemical polymerization [19–23], electrogeneration (electro deposition) of CP on CNT electrodes [24–27] or electrochemical co-deposition from a monomeric solution with dispersed CNTs forming a thin composite coating the electrode [28–34]. The dispersion of CNTs in the monomeric solution has been achieved by the utilization of ionic liquids [35], acidic treatment of the CNT [29,36–39] and the utilization of surfactants [32,34,40]. The surfactant sodium dodecylbenzenesulfonate (NaDBS) disperses CNTs at a high degree in aqueous solution [41–44] and can be utilized in addition as supporting electrolyte for the electrochemical co-deposition process. Thin films (<15 μm) of the composite of polypyrrole, carbon nanotubes and dodecylbenzenesulfonate, PPy-DBS-MWCNT, have been electrogenerated [32,34]. The morphology, electronic conductivity and the thermal stability of self-supported PPy-DBS-MWCNT electrode were studied [32] and the electrochemical and mechanical properties of PPy-DBS-MWCNT on ITO electrode were investigated [34].

In this paper, the general electrochemical conditions for the galvanostatic and potentiostatic synthesis of thick films (>15 μm) of the composite PPy-DBS-MWCNT are determined. The films are removed from the metal electrode and used as self-supported electrodes for their electrochemical characterized via consecutive potential cycles and consecutive square potential waves. The degradation process of the material electroactivity is followed in $NaClO_4$ aqueous solution for different anodic and cathodic potentials. Conformational and structural changes inside the material driven by the electrochemical reactions are studied.

* Corresponding author.
E-mail addresses: toribio.fotero@upct.es (T.F. Otero), jschumacher@arquimea.com (J. Schumacher).

http://dx.doi.org/10.1016/j.jelechem.2016.10.018
1572-6657/

2. Materials and methods

2.1. Chemicals

Pyrrole (Fluka) was distilled under vacuum using a diaphragm vacuum pump and stored at −10 °C. Multi-walled carbon nanotubes (MWCNT) (Sigma-Aldrich, purity >90%, outer diameter 10–15 nm, inner diameter 2–6 nm, length 0.1–10 μm), sodium perchlorate ($NaClO_4$) (Sigma-Aldrich) and sodium dodecylbenzenesulfonic acid (NaDBS) salt (Sigma-Aldrich) were used as received. All aqueous solutions were prepared with ultrapure water from Millipore Milli-Q equipment.

2.2. Equipment and experimental conditions

The electrochemical experiments were performed using an Autolab potentiostat/galvanostat PGSTAT302 controlled by NOVA 1.11 software. The electrochemical measurements were carried out in 0.1 M $NaClO_4$ aqueous solutions with a three electrode one-compartment electrochemical cell using an Ag/AgCl (3 M KCl) reference electrode (RE) from Metrohm and stainless steel (AISI 316) plates as counter electrodes (CE). The total mass of dried electropolymerized film was determined with a Sartorius SC2 balance (±0.1 mg) from the mass difference between the coated and uncoated electrodes. Microscopic pictures were attained from a scanning electron microscopy equipment (SEM, Hitachi S-3500N microscope) with electron energy of 5 kV. The thickness of the electrogenerated films was determined using a Helios Preisser digital micrometer (±1 μm) after peeling-off from the working electrode.

2.3. Film preparation

The composite PPy-DBS-MWCNT films were electrogenerated at room temperature from 0.1 wt% MWCNT, 0.03 M NaDBS and 0.1 M pyrrole aqueous solutions. The MWCNT were dispersed in a 0.03 M NaDBS aqueous solution in an ultrasonic bath for 1 h. Then 0.1 M pyrrole was added and the monomeric solution was prepared using the magnetic stirrer for 30 min at 60 rpm. Preliminary studies of the monomeric solution and the synthesis were conducted in a three-electrode electrochemical cell. The working electrode (WE) was a stainless steel plate. The WE with a surface area of 900 mm^2 (2 × 30 mm × 15 mm) was placed symmetrically between two parallel stainless steel plates with the same surface area (total area of 1800 mm^2), used as counter electrodes, at a distance of 1 cm. The immersed surface area of the WE and the CE were 600 mm^2 (2 × 20 mm × 15 mm) and 1200 mm^2 respectively. In this way a uniform electric field allowed the electropolymerization of two uniform films, one on each side of the WE, by oxidation-polymerization under constant potential.

2.4. Preparation of the self-supported PPy-DBS-MWCNT electrodes

Once electrogenerated, rinsed and dried, the electrogenerated films (each 13.92 mg and 300 mm^2) were peeled off from the WE. Then each film was cut to produce longitudinal strips, 2 mm width and 20 mm length. Taking one of these new films a transverse narrow (1 mm) paint strip was painted on both sides at 13 mm from the bottom and at 6 mm from the top. The clamp electrical contact was connected at the top of the film and the film electrode was immersed with the electrolyte meniscus below the transverse paint strip. The transversal paint strip closes polymer pores avoiding the electrolyte capillarity towards the metallic clamp. The immersed area of the PPy-DBS-MWCNT electrode in the electrolyte (below the transversal paint strip) was 16 mm^2, corresponding to an electroactive mass of 1.2 mg. Fig. 1 presents the self-supported PPy-DBS-MWCNT film prepared to be used as WE for the electrochemical characterization.

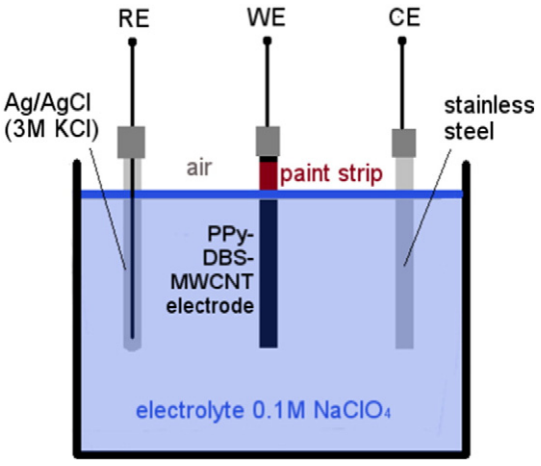

Fig. 1. Experimental set-up for electrochemical characterization: one compartment electrochemical cell with Ag/AgCl reference electrode (RE), bilayer muscles as working electrode (WE) and stainless steel counter electrode (CE).

3. Results and discussion

3.1. Electrochemical synthesis

3.1.1. Electrolyte potential window

Preliminary studies have been conducted in order to determine the electrolyte potential window, the potential where the monomer oxidation-polymerization starts on the clean WE and both, the potential range and current range for the oxidation-polymerization in presence of the MWCNT with a minimum interference of the electrolyte discharge.

The electrolyte potential window was determined by submitting the steel WE to consecutive potential cycles at 15 mV s^{-1} between −1400 mV and 1600 mV, in the background electrolyte (0.03 M NaDBS aqueous solution). The voltammetric response shows (Fig. 2a, red dashed line), that under the studied experimental conditions the electrolyte potential window (potential range where the electrochemical reactions are absent) ranges from −1250 mV until 1250 mV.

3.1.2. Monomer oxidation potential without and with MWCNT in solution

By repeating the voltammetric cycle, now in presence of the pyrrole monomer (0.03 M NaDBS and 0.1 M pyrrole aqueous solution) the voltammetric response shows (Fig. 2a, blue line) that the pyrrole oxidation-polymerization starts at 690 mV forming a brown film on the WE. By reversing the potential sweep higher oxidation-polymerization currents are observed at the beginning of the cathodic potential sweep than those attained during the previous anodic potential sweep originating a characteristic nucleation voltammetric loop. At more cathodic potentials than −500 mV the reduction of the electrogenerated film is initiated giving a reduction maximum at −1070 mV.

Using a clean cell, clean electrodes and a fresh 0.03 M NaDBS, 0.1 M pyrrole and 0.1 wt% MWCNT aqueous solution the oxidation-polymerization begins (Fig. 2a, inset green line) at 620 mV. A black film is formed on the electrode giving a nucleation loop when the potential sweep is reversed. The current flowing by the WE during the full oxidation-polymerization-nucleation loop is higher than that observed in absence of the MWCNT. The electrogenerated composite (Fig. 2a, green line) presents higher reduction currents at lower reduction potentials than the reduction of the PPy-DBS (Fig. 2a, blue line) giving a reduction maximum at −950 mV.

Beyond the potential of the monomer oxidation higher currents flow through the system in presence of MWCNT: more monomer arrives to the WE per unit of time, probably adsorbed on the MWCNT-DBS units.

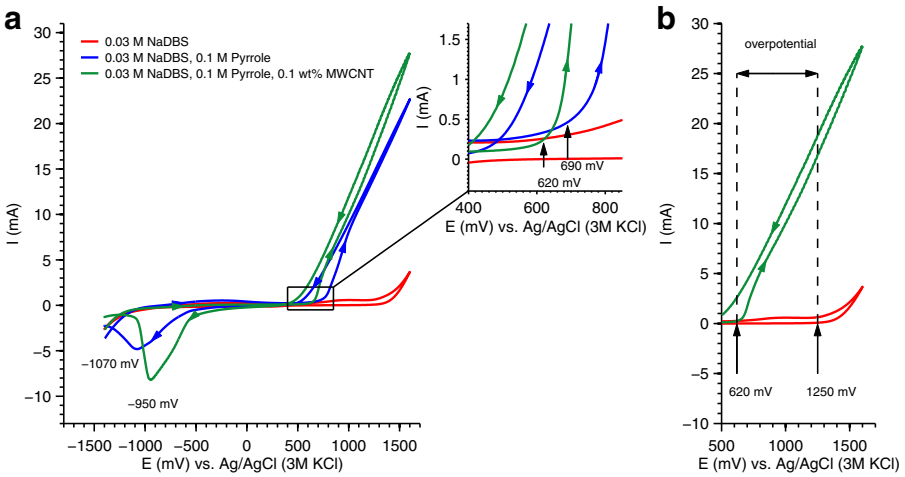

Fig. 2. Monomeric oxidation potential: (a) Voltammetric responses of the first potential cyclic of 0.03 NaDBS (red), 0.03 M NaDBS, 0.1 M Pyrrole (blue) and 0.03 M NaDBS, 0.1 M Pyrrole, 0.1 wt% MWCNT aqueous solution, monomeric oxidation potential (inset) without MWCNT (blue) at 690 mV and with MWCNT (green) at 620 mV (b) monomeric oxidation potential window (620 mV, 1250 mV) without discharge of the electrolyte.

By comparing the potential window of the supporting electrolyte with the monomer oxidation potential, the useful potential window for the monomer oxidation-polymerization goes from 620 mV (beginning of the monomer oxidation-polymerization) to 1250 mV, where the electrolyte discharge starts (Fig. 2b). In that potential range the generation of PPy-DBS-MWCNT composites is expected to occur in absence of parallel electrolyte oxidation. Fig. 2b also indicates that the composite could be electrogenerated in absence of electrolyte oxidation under galvanostatic control using lower current densities than 2.83 mA cm^{-2} (up to 17 mA flow through the 600 mm^2 of the steel electrode surface inside the oxidation-polymerization potential window before starting the electrolyte discharge).

The high current range could be explained by the increase of the electroactive area when MWCNTs are present. The MWCNTs adsorbs the NaDBS surfactant becoming negatively charged and therefore being attracted by the WE at anodic potentials. The MWCNTs attach to the WE acting as template for the polymer depositing [20] resulting in thicker and rougher films compared to smooth PPy-PO_4 and PPy-DBS films [34]. The surface area of the material growing on the WE is greater in presence of the MWCNTs than during the monomeric polymerization in absence of MWCNTs. As a consequence, for the same potential higher currents flow in presence of MWCNTs.

3.1.3. Electrogeneration of thick self-supported polymer films

Thick films of the PPy-DBS-MWCNT composite were generated using a clean cell, clean electrodes and a fresh solution by applying −0.2 V for 1 s and then stepping the potential to 0.8 V for 3600 s. Fig. 3 presents the chronoamperometric (current-time) and chronocoulometric (charge-time) responses recorded during the synthesis. The chronoamperometric response (Fig. 3a) shows the characteristic shape of the synthesis at constant potential [2,45] initiated by nucleation and growth of the polymer: see the characteristic nucleation chronoamperometric minimum at short times (Fig. 3a inset).

The initial sharp maximum is due to the charge of the electrical double layer (EDL) at the electrode-electrolyte interface. Thus the chronoamperometric response indicates the formation, growth and coalescence of polymeric nuclei [46]. Here, the chronoamperometric response shows for long polymerization times an irregular evolution of the flowing current (Fig. 3). This could be related to changes of the surface area of the WE during synthesis due to MWCNT incorporation. By integration of the chronoamperometric response the consumed charge during the electrochemical synthesis (polymerization process) is gained (Fig. 3b). The overall charge consumed during the synthesis was 20.62C.

After electrogeneration the coated WE was rinsed several times with ultrapure water and dried in air for one day. The polymer mass,

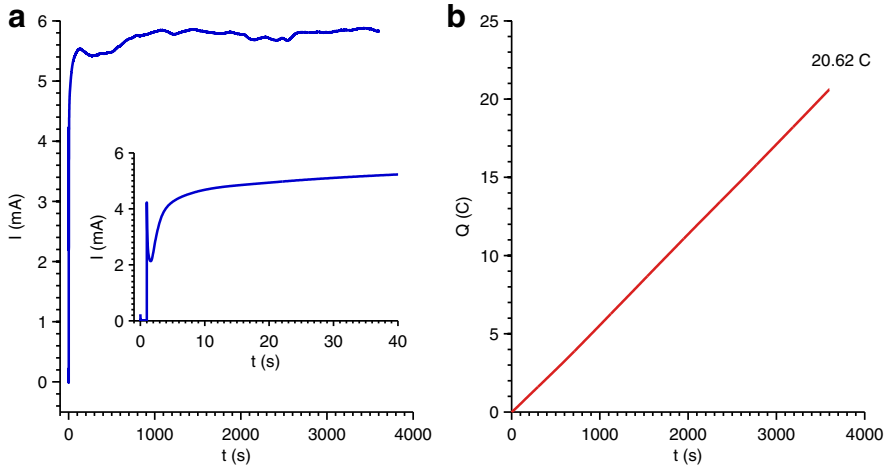

Fig. 3. Chronoamperogram and Chronocoulogram recorded during synthesis of the thick PPy-DBS-MWCNT composite film at constant potential at −0.2 V for 1 s and 0.8 V for 3600 s. (a) chronoamperometric response with inset: enlargement of the chronoamperogram for the first seconds (b) chronocoulometric response with a final consumed charge of 20.62C.

determined by mass difference between that of the uncoated and coated electrode, was 27.8 mg with a total area of 600 mm^2. By scrapping the electrode borders two separate films were peeled off, one per electrode face, with an estimated mass of 13.92 mg each. The average film thickness was 48.6 μm.

3.2. SEM microscopy

The SEM micrographs (Fig. 4a and b) show a cauliflower structure with some irregularities on the surface in contact with the monomeric solution. This could explain the non-uniform evolution of the current during the synthesis due to the non-uniform incorporation of the MWCNT to the growing film. Similar irregular morphologies were described for thin films of PPy-DBS-CNT composites synthesized by cyclic voltammetry [34] and constant potential [32]. The morphology of PPy-DBS films is unaffected by the electrochemical methodology used for the electrosynthesis presenting a smoother and more regular surface [47]. The cross section (Fig. 4b) presents a dense and compact structure of the bulk film like PPy-DBS-functionalized CNT films [39]. The surface in contact with the electrode during electropolymerization (Fig. 4b, inset right) shows a smooth even structure.

3.3. Stationary voltammetric responses: influence of the cathodic potential limit

The self-supported electrode was cycled in 0.1 M $NaClO_4$ aqueous solution between a fixed anodic potential limit of 0.8 V and rising cathodic potential limits (ranging from −0.4 V up to −2.5 V) at 10 mV s^{-1}. For each potential range the electrode was cycled until a stationary voltammetric response (consecutive voltammograms overlap) was reached (here after two cycles), eliminating any possible material memory [48,49]. Fig. 5a and c show, overlapped, the third stationary voltammetric responses until a different cathodic potential each indicated on the figures.

For more cathodic potential limits than −1 V, film oxidation and film reduction maxima are present (Fig. 5 a) at 0.167 V and −0.836 V respectively. The large anodic peak includes the oxidation of the two electroactive components (PPy and CNTs) of the film, which were also reported in aqueous solutions of lithium perchlorate and NaDBS [32]. Previous electrochemical studies in a smaller potential range (between −0.6 V and 0.1 V) and at higher scan rates (50–500 mV s^{-1}) of electrogenerated PPy-CNT films on metal electrodes in aqueous solution [29,37] reported several minor anodic and cathodic peaks and shoulders from the generated material. For potential ranges between −1 V and 1.1 V at 5 mV s^{-1} the voltammetric responses from thin films revealed also distinct anodic and cathodic maxima [34]. Under conditions akin to this study the voltammetric response of thick PPy-DBS films have a similar shape, but presenting a smaller potential separation between the anodic and the cathodic peak [50]. A smaller potential separation between both peaks was also reported for thinner PPy-MWCNT films [36].

Fig. 5c shows the stationary voltammetric responses from rising cathodic potential limits exceeding the material reduction maximum, ranging from −1 V to −2.5 V, to the same anodic potential limit of 0.8 V every time. After the material reduction maximum, the current converges zero. For rising cathodic potential limits the beginning of the film oxidation and the material oxidation maximum shift to higher anodic potentials with the parallel increase of the current at the maximum. Those responses correspond to more reduced states of the film because the current never drops to zero after the reduction maximum. This anodic shift of the film oxidation indicates that the beginning of the material oxidation requires higher overpotential (more electrochemical energy) for higher reduced materials [51]. Under present experimental conditions (constant temperature and constant electrolyte concentration) the only energetic source for the material oxidation is the applied oxidation overpotential. In this context results from Fig. 5 indicate that deeper reduced states of the material attained by potential sweep until higher cathodic potential limits present more stable energetic states, which require higher oxidation overpotentials to be re-oxidized. Any of those rising reduced and stable energetic states of the material is erased by its oxidation completion (overcoming the oxidation maximum) giving overlapped reduction voltammetric responses (Fig. 5c). In addition, any of those stable energetic states, and the associated anodic voltammetric response, is reproduced if after the oxidation maximum the next potential cycle is reversed at the concomitant cathodic potential limit.

3.4. Stationary coulovoltammetric responses

The voltammetric (I-E) responses from Fig. 5a and c give, by integration of the flowing current, the concomitant coulovoltammetric (Q-E) response depicted by Fig. 5b and d. The potentiostat and the software used here give directly voltammetric and coulovoltammetric responses. Positive charge increments are related to oxidation charges and negative charge increments account for reduction charges.

Whatever the cathodic potential limit the coulovoltammetric responses depict continuous charge variations driving faradaic reactions. For lower cathodic potential limits than −1 V the Q-E responses are (Fig. 5b) closed loops: the material oxidation charge equals the material reduction charges. Thus the charge increment from the maximum to the minimum accounts for the reversible charge (Q_{rev}) consumed by the reversible film oxidation/reduction. Each coulovoltammetric minimum from the closed loop was taken as zero charge origin in Fig. 5b and d in this way the figures show a visual evolution of the film reversible charge with the studied variables.

For higher cathodic potential limits than −1 V the Q-E response presents in addition to the closed loop an open part on the left side (Fig. 5d). The charge difference between the charge of the initial potential and that of the final potential (open part) is a net reduction charge, not recovered during the anodic sweep: this is an irreversible charge consumed by irreversible reduction reactions.

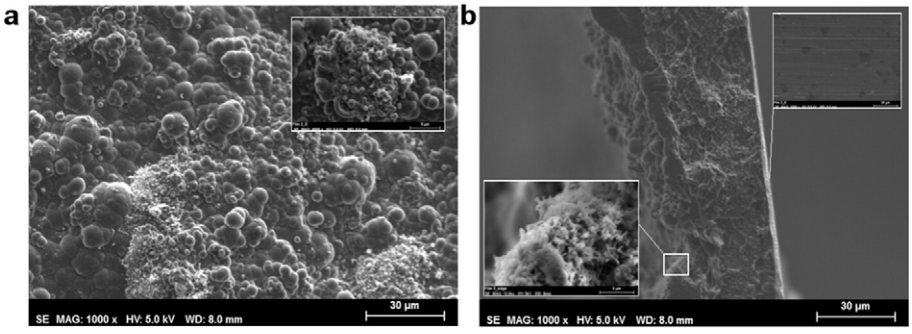

Fig. 4. SEM micrographs of the PPy-DBS-MWCNT film: (a) surface in contact with the monomeric solution during electropolymerization with irregularities (inset) (b) cross section of the thick film with porous areas (left inset) and surface in contact with the stainless steel electrode during electropolymerization (right inset).

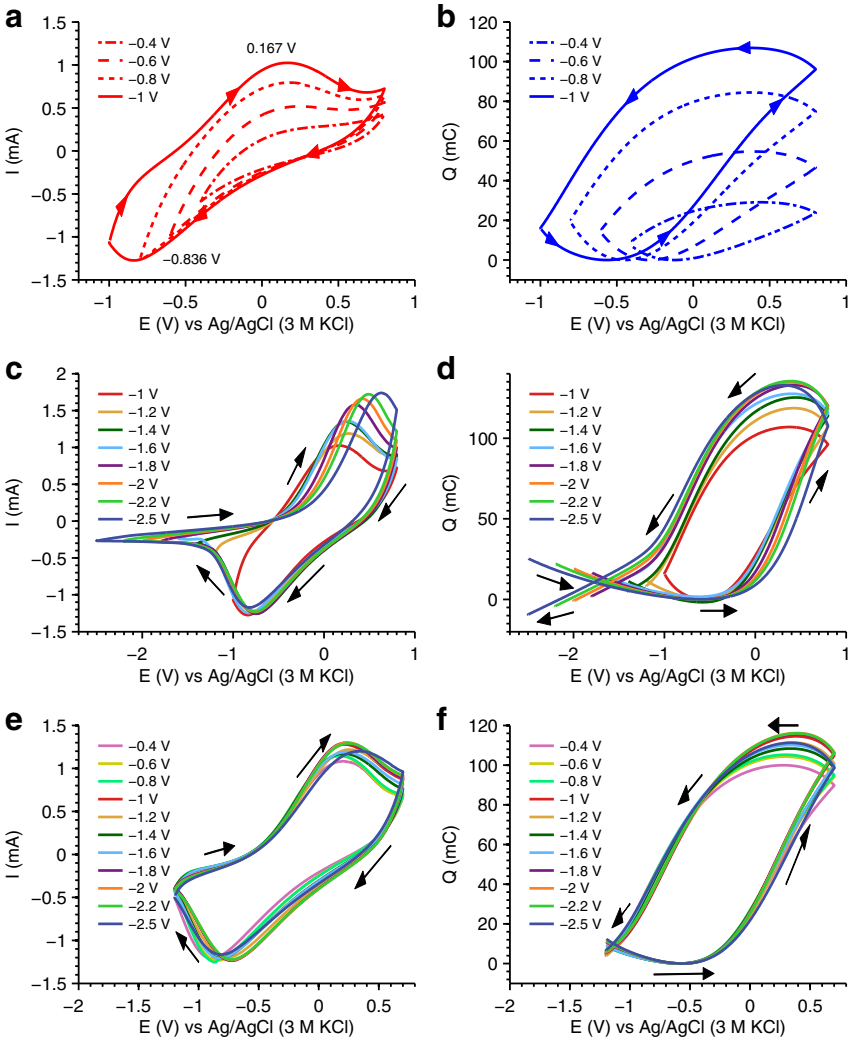

Fig. 5. Stationary voltammetric and coulovoltammetric response of the self-supported PPy-DBS-MWCNT electrode in 0.1 M $NaClO_4$ aqueous solution at 10 mV s^{-1} from the same anodic limit of 0.8 V to different cathodic potential limits: (a) cathodic potential limits ranging from −0.4 V to −1 V (b) contaminant coulovoltammetric response of cathodic potential limits ranging from −0.4 V to −1 V (c) different cathodic potential limits ranging from −1 V to −2.5 V (d) contaminant coulovoltammetric response of cathodic potential limits ranging from −1 V to −2.5 V (e) Stationary voltammetric controls between −1.2 V and 0.7 V after each experiment from Fig. 5a and c (f) contaminant coulovoltammetric responses.

Table 1 represents the evolution, as a function of the cathodic potential limit, of the charge consumed by the reversible film oxidation/reduction and that involved in parallel irreversible reduction reactions.

The reversible redox charge (Q_{rev}) increases with the cathodic potential limits up to −2.2 V and then decreases for the cathodic limit of −2.5 V. More cathodic potential limits result (Fig. 5b and d) in higher charges consumed to reduce the film but, simultaneously, the oxidation maximum shifts to higher anodic potentials interrupting the film oxidation before completion. For the potential cycle from −2.5 to 0.8 V the second effect prevails due to the shift of the anodic maximum interrupting the material oxidation before its completion.

Table 1
Evolution of the reversible (closed loop) and irreversible charge (open part) of the coulovoltammetric responses of voltammetric sweep from different cathodic limits.

Cathodic limit/V	Reversible charge Q_{rev}/mC	Irreversible charge Q_{irr}/mC
−0.4	29.11	−2.91
−0.6	54.70	−2.23
−0.8	84.47	−1.78
−1	106.92	−0.22
−1.2	118.62	3.59
−1.4	125.24	6.31
−1.6	127.55	4.29
−1.8	132.90	14.61
−2	134.52	20.04
−2.2	135.40	26.25
−2.5	132.79	34.73

At more cathodic potentials than −1 V irreversible reduction reactions are present consuming rising irreversible charge (Q_{irr}), Table 1, for higher cathodic potential limits. In the polymer blend PPy-DBS this irreversible reaction was ascribed to the hydrogen evolution from the HDBS component [52]. Self-supported polypyrrole films synthesized in presence of small inorganic counterions do not present any irreversible charge in aqueous solution until −3 V [53].

Thus the film reduction occurs (Fig. 5d and Table 1) beyond −1 V in parallel to some hydrogen evolution [53,54], which is strongly inhibited (Fig. 5b) by the electrode material but not avoided.

Summarizing Fig. 5b and d and Table 1 corroborate that the material reduction goes on beyond the voltammetric reduction maximum until −2.5 V giving higher reversible charges for more cathodic potential limits. Beyond −1 V the film reversible reduction overlaps irreversible reduction reactions attributed to the hydrogen evolution from the HDBS component. The irreversible charge consumed by this irreversible

reaction also increases for rising cathodic potential limits. The coulovoltammetric responses provide a good separation of those charges consumed by reversible and irreversible processes for each cathodic potential limit.

3.5. Voltammetric and coulovoltammetric control of the material electroactivity

After submitting the material to consecutive potential cycles for every cathodic potential limit the state of the material was checked by two consecutive cycles from −1.2 to 0.7 V at 10 mV s^{-1}. The stationary voltammetric responses (Fig. 5e) show: a good stability of the material and that the material memory of the energetic state written by the previous experiment at each cathodic potential limit has been erased. The control responses after cathodic potential limits higher than −1 V show a consumed charge of 114 mC (±6%). The reference responses for lower cathodic potential limits (<−1 V) show lower charges (114 mC (±10%)). When the charge of the voltammetric control after an experiment deviates over 6% related to that of the previous control the electrode was discarded and a fresh film electrode was used to go on the experimental series.

3.6. Stability of the film under extreme voltammetric conditions

In order to check how stable the PPy-DBS-MWCNT film is when submitted to potential cycles until high anodic or high cathodic potential limits, a PPy-DBS-MWCNT self-supported electrode was submitted to two consecutive cycles from −5 V to 1 V at 4 mV s^{-1} in 0.1 M $NaClO_4$ aqueous solution. Fig. 6a shows the attained voltammetric responses. Despite the high cathodic potential limit, the hydrogen evolution by direct water discharge on the electrode seems quite inhibited: the cathodic current keeps below 0.3 mA in the potential range from −2 V to −5 V. This flowing current indicates that the material keeps electroactive in that potential range, as corroborated by its subsequent oxidation during the anodic potential sweep, contradicting the conducting/insulator transition model after the reduction maximum [55–58]. Nevertheless, the irreversible hydrogen evolution, through the HDBS component, is present there (Fig. 7b). A small decrease of the reversible charge on the second voltammogram seems related to the partial oxidation completion during the first one (the oxidation maximum is not completed) and the concomitant partial erasing of the structural material memory stored at so high cathodic potential limits. The energetic structural memory written in the material at so high reduction overpotential shifts the oxidation voltammetric maximum from 0.167 V (Fig. 5a) to 0.69 V (Fig. 6a), as described for structural effects induced by reduction reactions at high cathodic potentials [59]. In the subsequent cycle the oxidation maximum is further shifted to 0.87 V.

Fig. 6b shows the two consecutive coulovoltammetric responses taken the minimum of the closed loop as zero reference for charges. The reversible charge of the film oxidation/reduction (closed loop) is 150 mC. Compared with a redox charge of 133 mC (Table 1) when the film was reduced until −2.5 V the conclusion is that the film reduction goes on, at a low reduction rate, until −5 V. The structural transformation of the material at so high cathodic potential during the initial sweep was not fully erased by oxidation completion during the first sweep with the subsequent decrease by 6.6% of the reversible charge on the second coulovoltammogram. This reduction overlaps beyond −1 V (see Section 3.3) a slow evolution of hydrogen, never observing a direct formation of bubbles on the electrode, consuming (Fig. 6b) over 380 mC until −5 V. As a partial conclusion the self-supported material presents a strong degradation resistance by polarization at very high cathodic potentials, up to −5 V, in aqueous solutions not experiencing noticeable degradation processes, keeping the film electroactivity and showing a remarkable inhibition of the water electrolysis with hydrogen release.

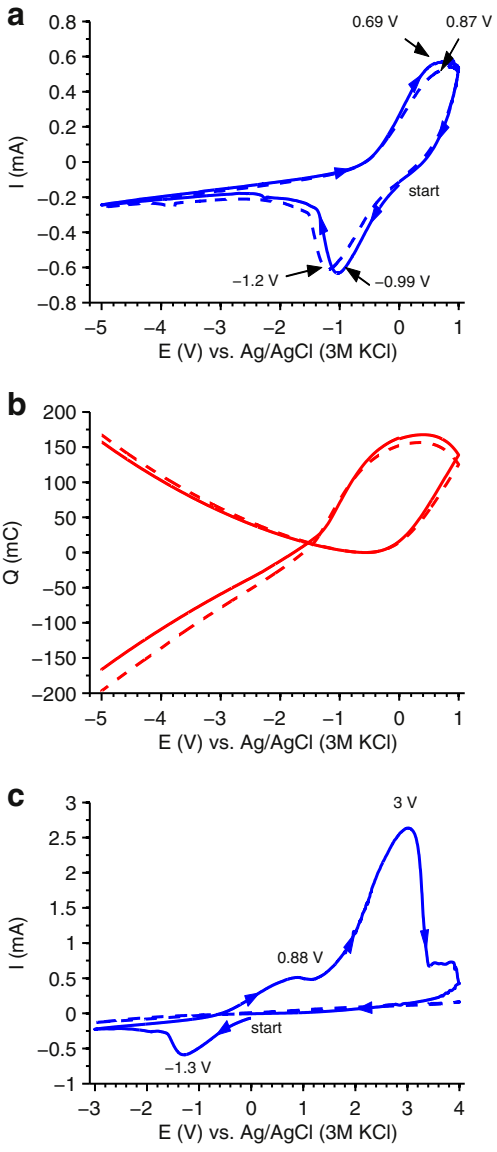

Fig. 6. Polymeric stability of PPy-DBS-MWCNT in 0.1 M $NaClO_4$ aqueous solution: first (continuous line) and second cycle (dashed line) at 4 mV s^{-1} (a) voltammetric responses between −5 V and 1 V (b) concomitant coulovoltammetric response (c) voltammetric responses in the potential range from −3 V to 4 V.

Keeping now the cathodic potential limit at −3 V the PPy-DBS-MWCNT electrode was submitted to consecutive potential cycles until 4 V. By starting the potential sweep from 0 V, Fig. 6c shows the attained voltammetric responses depicting a reduction peak at −1.3 V, and during the first cycle (continuous line) a first oxidation peak at 0.88 V and a second one at more anodic potentials (3 V). The second consecutive cycle (dashed line) shows a flat structure: both reduction and oxidation peaks vanish on the second voltammogram corroborating the full degradation of the material electroactivity by overoxidation during the second anodic peak of the first voltammogram. Degradation is used here in the sense of transformation of the material properties by any atmospheric, physical, chemical or electrochemical influence. Basic conducting polymers with small counterions also experience similar full degradation during the first anodic sweep [60]. PPy-DBS films present a high resistance to the overoxidation [50]. The PPy-DBS-MWCNT degradation maximum in 0.1 M $NaClO_4$ aqueous solution starts beyond 1.2 V that means at the same potential as the expected oxygen formation. Nevertheless, the degradation maximum occurs at 3 V a higher value than those reported for PPy-DBS and PPy synthesized from

$LiClO_4$ solutions [50,60] indicating a superior polymeric stability and degradation resistance of PPy-DBS-MWCNT.

3.7. Stationary chronoamperometric responses

In order to further investigate those structural and energetic changes produced in the material by reduction beyond the voltammetric maximum revealed from Fig. 5c the self-supported PPy-DBS-MWCNT material was submitted to consecutive square potential steps from a different reduction potential every time to the same oxidation potential. Every square potential step was repeated three times to ensure stationary anodic and cathodic chronoamperometric responses. The submission to a potential step from different reduced states (different cathodic potential) to the same oxidized state (constant anodic potential) and vice versa gives the empirical polymeric oxidation and reduction rates [61,62].

3.7.1. Square potential steps from different cathodic potentials

The self-supported PPy-DBS-MWCNT electrode was submitted to consecutive square potential steps from a different cathodic potential, selected in the potential range from −0.6 V to −2.5 V, kept for 300 s every time to the same anodic potential 0.7 V kept for 200 s. After two consecutive square potential waves stationary chronoamperometric responses are attained. Fig. 7a and c show overlapped these stationary oxidation and reduction, respectively, chronoamperometric responses. The anodic chronoamperometric responses from different reduced states, which were obtained by polarization for the same time at higher cathodic potentials, show a maximum characteristic of nucleation processes [51]. The maximum shifts to lower currents and higher oxidation times when the initial state was attained by reduction at more cathodic potentials. By integration of the chronoamperometric responses the chronocoulometric responses (Fig. 7b and d) are attained: they represent the evolution of the polymer oxidation (Q/we^- is the specific, per unit of dry polymer mass, w, concentration of polymeric active centers, Q/e^-, being e^- the electron charge). Thus Fig. 7b illustrates that slower initial oxidation rates (initial Q/E slopes) are attained from deeper reduced initial states, which means from higher initial concentrations of polymeric active centers. According with the electrochemically stimulated conformational relaxation (ESCR) model [51] these apparently anomalous electrochemical responses (chemical and electrochemical kinetics from present textbooks predict higher oxidation rates from rising initial concentrations of the reactant) can be explained by reaction-driven conformational and structural changes in the bulk polymer [63–66].

The film reduction back to the studied cathodic potential limit shows chronoamperometric responses, Fig. 7c, depicting several shoulders

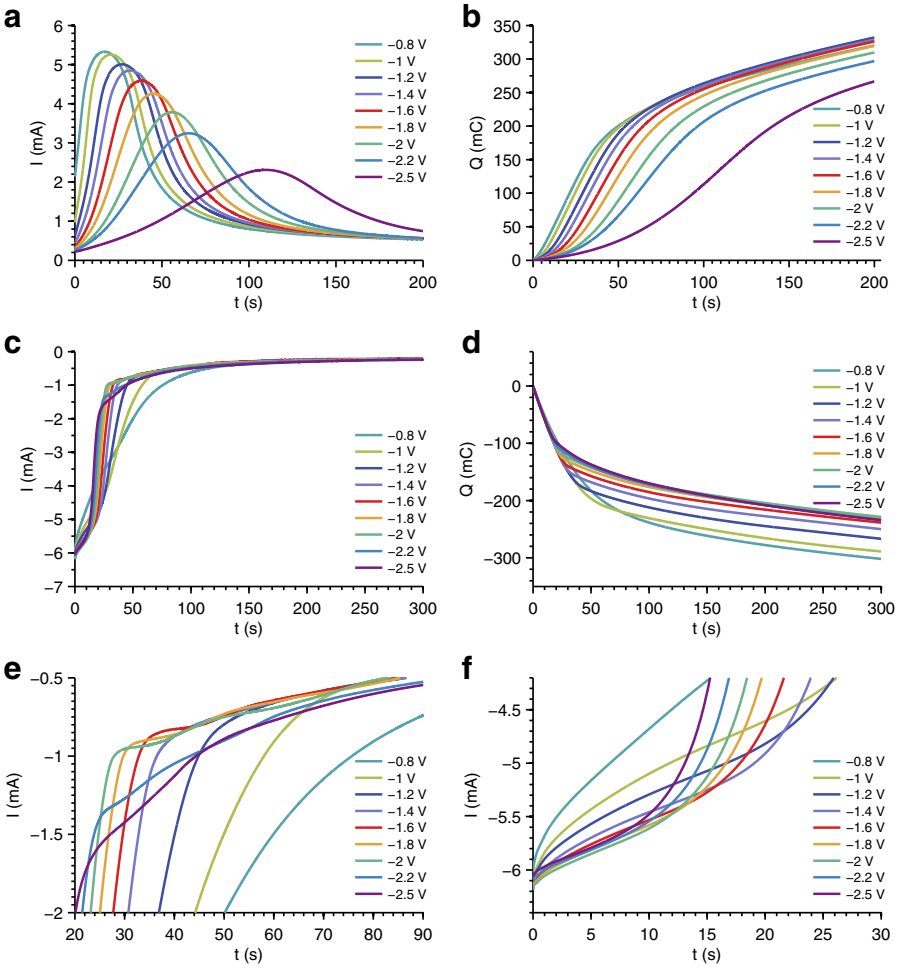

Fig. 7. Stationary chronoamperometric responses (after two consecutive potential waves) from self-supported PPy-DBS-MWCNT electrodes in 0.1 M NaClO4 aqueous solution submitted to consecutive square potential waves (a) oxidation by potential steps from different cathodic potentials indicated on the figure held for 300 s each to the same anodic potential 0.7 V, held for 200 s (b) chronocoulometric responses during oxidation (c) reduction by potential step back to the cathodic potential (d) chronocoulometric responses during reduction (e) detail of inflection area of the chronoamperometric response (f) detail of the chronoamperometric response at short reduction times.

(Fig. 7e) that should indicate the presence of different reduction-driven structural changes in the film. A decrease in the slope (reduction rate) at short reduction times is observed for rising reduction potentials (Fig. 7f). Similar cathodic chronoamperometric responses where obtained with PPy-HpPS [67] and PPy-DBS also showing new structural changes still not described by the ESCR model [53].

3.8. Description of the electrochemical responses by driving reactions

CNT follow oxidation/reduction processes in aqueous solution [68–70] driving the exchange of cations [70]. PPy-DBS films also oxidize and reduce in a reversible way in the same electrolyte with exchange of cations [71]. Thus, the PPy-DBS-MWCNT composite film includes two different active centers: CNT* and PPy*, understood as those points where a positive charge will be stored after oxidation. Each of the constituent active centers will follow its specific electrochemical reaction [72]:

$$PPy * CNT * \left(DBS^{-}Na^{+}\right)_{n} \rightleftharpoons PPy * CNT^{n+}\left(DBS^{-}\right)_{n} + n\left(Na^{+}\right) + ne^{-} \quad (1)$$

$$PPy * CNT * *\left(DBS^{-}Na^{+}\right)_{n} \rightleftharpoons PPy^{n+}CNT^{*}\left(DBS^{-}\right)_{n} + n\left(Na^{+}\right) + ne^{-} \quad (2)$$

DBS^{-} represents the anion trapped during the film electrogeneration, Na^{+} is the cation penetrating in the composite electrode from the electrolyte during the electrode reduction (reactions (1) and (2) backwards) and required to compensate the negative charge on the macroions DBS^{-}. According with the voltammetric and chronoamperometric responses both reactions overlap on a large potential range of the voltammetric maxima. The film reduction should drive the Faradaic entrance of cations for charge balance: the electrode must swell generating the required free volume to lodge those coming ions. The film oxidation should drive the film shrinking by expulsion of cations towards the solution. Those macroscopic structural changes driven by the reactions have been described by the ESCR model [73]. In addition other structural changes can be driven by the reaction and coulovoltammetric responses are considered as one of the most efficient ways to reveal them [53,54,74].

3.9. Reaction-driven structural changes from coulovoltammetric responses

Analysis of coulovoltammetric responses of CPs showed several slope variations. Those Q/E slopes determine the reaction rate [54]:

$$\Delta Q[C]/\Delta E[V] = \left(\Delta Q[C] * V\left[Vs^{-1}\right]\right)/\left(w[g] * z\left[Eq\,M^{-1}\right] * F\left[C\,Eq^{-1}\right] * \Delta E[V]\right) = (\Delta Q * v)/(w * z * F\Delta E)\left[Mg^{-1}s^{-1}\right] \quad (3)$$

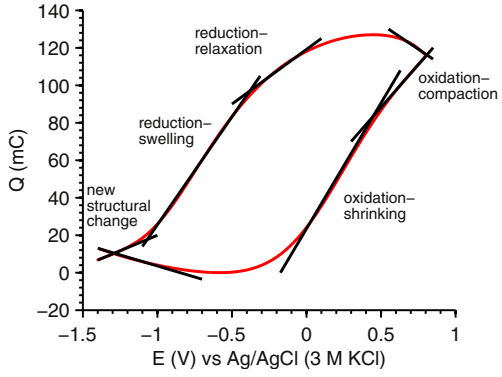

Fig. 8. Coulovoltammetric response of the self-supported PPy-DBS-MWCNT electrode in 0.1 M $NaClO_4$ aqueous solution at 10 mV s^{-1} in the potential range of −1.4 V to 0.8 V with slope variation associated to structural changes in the material.

Where w is the mass of electroactive composite reacting inside the solution, z is the ion charge, F is the Faraday constant and ν is the experimental potential sweep rate. Thus the slope is the specific (per unit of mass) reaction rate and any slope variation indicates a change of the composite reactions' rates. Considering that only reversible reactions (1) and (2) occur in the studied potential ranges any slope variation must be due to a reaction-driven structural change inside the material [53,54]. Fig. 8 shows the coulovoltammetric response in the potential range from −1.4 V to 0.8 V.

At the Q-E minimum the PPy-DBS-MWCNT presents its most reduced-swollen state. From there the material oxidation starts at increasing oxidation rates keeping then a high oxidation rate between 0 V and 0.45 V related to the fast oxidation-shrinking above described. But at 0.45 V the structure closes (the average distance between the electroactive centers in the film equals the diameter of the escaping cations trapping a great percentage of the cations involved in the redox process inside the film). The material oxidation-compaction goes on at so high overpotentials but now at a slower oxidation rate: the slope decreases. The system is outside the electrochemical equilibrium and the oxidation-compaction goes on at the beginning of the reduction process until the Q-E maximum. These oxidation-compaction processes give stable conformational energetic states of each of the two electroactive species present in the composite material. Those conformational energetic states should be the origin of the shoulders observed on the reduction chronoamperometric responses (Fig. 7c).

After the Q-E maximum the material reduction starts by slow relaxation of the compacted structures, generating the required free volume to lodge the cations penetrating from the solution for the required charge balance (reactions (1) and (2) backwards). Once the packed structures are relaxed the fast reduction-swelling (high slope) of the composite goes on. Nevertheless, before completion of the reduction-swelling process the reduction rate (the Q/E slope) decreases again. This slow reduction process was attributed to the formation, beyond a concentration threshold of cations and water inside the material, of small vesicles or lamellas constituted by water and cations surrounded by a monolayer of DBS^{-} and deep reduced and packed PPy [53]. Due to those slow structural changes the system is outside its electrochemical equilibrium and the growth of those new vesicular or lamellar structures goes on at the beginning of the anodic potential sweep until the coulovoltammetric minimum.

Based on those structural changes chronoamperometric responses from Fig. 7a and c can be rationalized. By oxidation at the same anodic potential every time the same oxidized-compacted structure is attained, which by reduction at rising overpotentials (Fig. 5c) gives faster reduction-relaxation processes. The oxidation-relaxation begins by nucleation of the cation entrance through those points of the composite/electrolyte interface having a higher mobility of both, polymer chains and CNTs. As a result, the concomitant shoulders are observed on the cathodic chronoamperometric responses.

On the other side, by reduction at rising cathodic potentials more vesicles or lamellas grow inside the material surrounded by deep reduced polypyrrole. Those are quite stable energetic structures. The subsequent oxidation starts by nucleation-relaxation of the deep reduced and conformational compacted PPy surrounding each vesicular or lamellar structures with entrance of the DBS^{-} from the lamellar membrane and expulsion of cations towards the solution (reactions (1) and (2) forwards). This requires extra energy. When the oxidation occurs under potential cycling the only energetic source (working under constant temperature, constant thermal energy, and constant electrolyte concentration, constant chemical energy) is the anodic overpotential: higher anodic overpotentials are required to oxidize (initial oxidation potential and oxidation peak) the new lamellar or vesicular structures attained by reduction at higher cathodic potential limits (Fig. 5c and d). Related to the oxidation branch of the chronoamperometric responses (Fig. 7a and b) the entrance of those large counterions in the surrounding packed conformational PPy requires longer oxidation

times for rising packed structures of the PPy by reduction at higher cathodic potentials.

Before those reaction-driven structural changes were included to explain electrochemical responses, voltammetric or chronoamperometric responses like those presented by Figs. 5 and 7 from conducting polymers [75], carbon nanotubes [69,76–78], graphene [79,80], porphyrin monolayers [81], and other organic electroactive materials were considered anomalous electrochemical responses. They were considered anomalous because deeper reduced initial states (higher concentrations of the reactant) give subsequent slower oxidation rates, contradicting the chemical kinetic rules. They were attributed to memory effects [75,82,83], relaxation effects [84–87], first cycles effects [88], and so on.

4. Conclusion

The electrochemical synthesis of thick PPy-DBS-MWCNT films can be performed under potentiostatic conditions between 0.65 V to 1.4 V and galvanostatic conditions using lower current densities than 2.83 mA cm^{-2} in the absence of parallel electrolyte discharge. Films having a thickness of 48.6 μm can be synthesized at constant potential and peeled off from the stainless steel electrode for the construction of free-standing PPy-DBS-MWCNT electrodes. The synthesized PPy-DBS-MWCNT film shows a dense and compact cauliflower structure with porous irregularities. When submitted to consecutive potential cycles the voltammetric responses indicate ionic exchanges driven by reversible redox reactions. Like other composite or blends incorporating DBS anions, PPy-DBS-MWCNT has a high stability in aqueous solution and reversible redox reactions occur until high cathodic potential limits (up to −5 V). Nevertheless, beyond cathodic potential limits of −1 V concurrent hydrogen evolution is present at a slow rate, only detected and quantified, by the consumed charge, from the coulovoltammetric responses. The composite is an excellent inhibitor of the water electrolysis. The hydrogen evolution was attributed to the HDBS component of the composite, not originating parallel pH changes in the film and, consequently avoiding the material degradation at so high cathodic potentials.

Overoxidation causes the degradation of the material electroactivity. At the anodic potential limit of 1.2 V the oxidative degradation of the composite is initialized. The material also presents a high resistance to the overoxidation, given that the degradation maximum is shifted until 3 V. Once this maximum is overcome the result is an irreversible full degradation of the material electroactivity.

Electrochemical responses (chronoamperometric, voltammetric) reveal reaction driven structural changes described by the ESCR model. In addition, new structural changes during oxidation were identified resulting in inertia effects and hinder a complete reduced structure. In $NaClO_4$ aqueous solution the PPy-DBS-MWCNT film shrinks during oxidation with closing and compaction of the structure and undergoes relaxation and swelling by reduction with formation of new (possibly lamellar or vesicular) structures beyond a reduction threshold.

Acknowledgement

This project has received funding from the European Union's Horizon 2020 research and innovation program under the Marie Sklodowska-Curie grant agreement no. 641822.

References

[1] E. Smela, Adv. Mater. 15 (2003) 481–494.
[2] T.F. Otero, Conducting Polymers, The Royal Society of Chemistry, 2016.
[3] L. Bay, T. Jacobsen, S. Skaarup, K. West, J. Phys. Chem. B 105 (2001) 8492–8497.
[4] E. Smela, N. Gadegaard, Adv. Mater. 11 (1999) 953–957.
[5] K. Kaneto, K. Yoshino, Y. Inuishi, Jpn. J. Appl. Phys. 22 (1983) L412.
[6] T.F. Otero, J.G. Martinez, Adv. Funct. Mater. 24 (2014) 1259–1264.
[7] T.F. Otero, Conducting Polymers: Bioinspired Intelligent Materials and Devices, Royal Society of Chemistry, 2015.
[8] A.F. Diaz, K.K. Kanazawa, G.P. Gardini, J. Chem. Soc. Chem. Commun. (1979) 635–636.
[9] F. Fusalba, P. Gouérec, D. Villers, D. Bélanger, J. Electrochem. Soc. 148 (2001) A1–A6.
[10] J. Bobacka, A. Lewenstam, A. Ivaska, J. Electroanal. Chem. 489 (2000) 17–27.
[11] P. Gómez-Romero, M. Lira-Cantú, Adv. Mater. 9 (1997) 144–147.
[12] S. Maw, E. Smela, K. Yoshida, R.B. Stein, Synth. Met. 155 (2005) 18–26.
[13] X. Wang, E. Smela, J. Phys. Chem. C 113 (2008) 369–381.
[14] J. Causley, S. Stitzel, S. Brady, D. Diamond, G. Wallace, Synth. Met. 151 (2005) 60–64.
[15] H. Karami, M.F. Mousavi, Talanta 63 (2004) 743–749.
[16] E. Frackowiak, F. Beguin, Carbon 39 (2001) 937–950.
[17] Q.-Y. Li, Z.-S. Li, L. Lin, X. Wang, Y.-F. Wang, C.-H. Zhang, H.-Q. Wang, Chem. Eng. J. 156 (2010) 500–504.
[18] J.G. Martínez, T. Sugino, K. Asaka, T.F. Otero, ChemPhysChem 13 (2012) 2108–2114.
[19] K. Lota, V. Khomenko, E. Frackowiak, J. Phys. Chem. Solids 65 (2004) 295–301.
[20] J. Fan, M. Wan, D. Zhu, B. Chang, Z. Pan, S. Xie, J. Appl. Polym. Sci. 74 (1999) 2605–2610.
[21] M. Cochet, W.K. Maser, A.M. Benito, M.A. Callejas, M.T. Martínez, J.-M. Benoit, J. Schreiber, O. Chauvet, Chem. Commun. (2001) 1450–1451.
[22] H. Zengin, W. Zhou, J. Jin, R. Czerw, D.W. Smith, L. Echegoyen, D.L. Carroll, S.H. Foulger, J. Ballato, Adv. Mater. 14 (2002) 1480–1483.
[23] J.-H. Kim, A.K. Sharma, Y.-S. Lee, Mater. Lett. 60 (2006) 1697–1701.
[24] C. Downs, J. Nugent, P.M. Ajayan, D.J. Duquette, K.S. Santhanam, Adv. Mater. 11 (1999) 1028–1031.
[25] N. Ferrer-Anglada, M. Kaempgen, S. Roth, Phys. Status Solidi B 243 (2006) 3519–3523.
[26] Y. Fang, J. Liu, D.J. Yu, J.P. Wicksted, K. Kalkan, C.O. Topal, B.N. Flanders, J. Wu, J. Li, J. Power, Sources 195 (2010) 674–679.
[27] J. Zeng, W. Wei, L. Wu, X. Liu, K. Liu, Y. Li, J. Electroanal. Chem. 595 (2006) 152–160.
[28] G.Z. Chen, M.S. Shaffer, D. Coleby, G. Dixon, W. Zhou, D.J. Fray, A.H. Windle, Adv. Mater. 12 (2000) 522–526.
[29] C. Peng, J. Jin, G.Z. Chen, Electrochim. Acta 53 (2007) 525–537.
[30] M. Hughes, G.Z. Chen, M.S. Shaffer, D.J. Fray, A.H. Windle, Compos. Sci. Technol. 64 (2004) 2325–2331.
[31] M. Wu, G.A. Snook, V. Gupta, M. Shaffer, D.J. Fray, G.Z. Chen, J. Mater. Chem. 15 (2005) 2297–2303.
[32] G. Han, J. Yuan, G. Shi, F. Wei, Thin Solid Films 474 (2005) 64–69.
[33] J. Zeng, X. Gao, W. Wei, X. Zhai, J. Yin, L. Wu, X. Liu, K. Liu, S. Gong, Sensors Actuators B Chem. 120 (2007) 595–602.
[34] J. Hernández-Ferrer, A. Ansón-Casaos, M.T. Martínez, Electrochim. Acta 64 (2012) 1–9.
[35] X. Lin, Y. Xu, Electrochim. Acta 53 (2008) 4990–4997.
[36] M. Hughes, G.Z. Chen, M.S. Shaffer, D.J. Fray, A.H. Windle, Chem. Mater. 14 (2002) 1610–1613.
[37] Y. Lu, T. Li, X. Zhao, M. Li, Y. Cao, H. Yang, Y.Y. Duan, Biomaterials 31 (2010) 5169–5181.
[38] J. Wang, Y. Xu, X. Chen, X. Sun, Compos. Sci. Technol. 67 (2007) 2981–2985.
[39] J. Wang, Y. Xu, F. Yan, J. Zhu, J. Wang, F. Xiao, J. Solid State Electrochem. 14 (2010) 1565–1575.
[40] P.-C. Ma, N.A. Siddiqui, G. Marom, J.-K. Kim, Compos. Part Appl. Sci. Manuf. 41 (2010) 1345–1367.
[41] A. Anson-Casaos, J.M. Gonzalez-Dominguez, M.T. Martinez, Carbon 48 (2010) 2917–2924.
[42] A.J. Blanch, C.E. Lenehan, J.S. Quinton, J. Phys. Chem. B 114 (2010) 9805–9811.
[43] M.F. Islam, E. Rojas, D.M. Bergey, A.T. Johnson, A.G. Yodh, Nano Lett. 3 (2003) 269–273.
[44] J. Liu, A.G. Rinzler, H. Dai, J.H. Hafner, R.K. Bradley, P.J. Boul, A. Lu, T. Iverson, K. Shelimov, C.B. Huffman, Science 280 (1998) 1253–1256.
[45] J. Arias-Pardilla, T.F. Otero, R. Blanco, J.L. Segura, Electrochim. Acta 55 (2010) 1535–1542.
[46] B.J. Hwang, R. Santhanam, Y.-L. Lin, J. Electrochem. Soc. 147 (2000) 2252–2257.
[47] S. Shimoda, E. Smela, Electrochim. Acta 44 (1998) 219–238.
[48] J. Heinze, A. Rasche, J. Solid State Electrochem. 10 (2006) 148–156.
[49] M.A. Vorotyntsev, M. Skompska, E. Pousson, J. Goux, C. Moise, J. Electroanal. Chem. 552 (2003) 307–317.
[50] L. Valero, J. Arias-Pardilla, M. Smit, J. Cauich-Rodríguez, T.F. Otero, Polym. Int. 59 (2010) 337–342.
[51] T.F. Otero, H. Grande, J. Rodriguez, Synth. Met. 76 (1996) 285–288.
[52] L. Valero, J.G. Martinez, T.F. Otero, J. Solid State Electrochem. 19 (2015) 2683–2689.
[53] T.F. Otero, J.G. Martinez, M. Fuchiwaki, L. Valero, Adv. Funct. Mater. 24 (2014) 1265–1274.
[54] T.F. Otero, M. Alfaro, V. Martinez, M.A. Perez, J.G. Martinez, Adv. Funct. Mater. 23 (2013) 3929–3940.
[55] N. Gospodinova, L. Terlemezyan, Prog. Polym. Sci. 23 (1998) 1443–1484.
[56] G. Inzelt, M. Pineri, J.W. Schultze, M.A. Vorotyntsev, Electrochim. Acta 45 (2000) 2403–2421.
[57] A. Pron, P. Rannou, Prog. Polym. Sci. 27 (2002) 135–190.
[58] J. Heinze, B.A. Frontana-Uribe, S. Ludwigs, Chem. Rev. 110 (2010) 4724–4771.
[59] T.F. Otero, H. Grande, J. Rodríguez, J. Phys. Chem. B 101 (1997) 8525–8533.
[60] T.F. Otero, M.J. Ariza, J. Phys. Chem. B 107 (2003) 13954–13961.
[61] T.F. Otero, J.M.G. de Otazo, Synth. Met. 159 (2009) 681–688.
[62] T.F. Otero, J. Arias-Pardilla, E. Chermak, Synth. Met. 160 (2010) 425–431.
[63] T.F. Otero, H.J. Grande, J. Rodriguez, J. Phys. Chem. B 101 (1997) 3688–3697.
[64] T.F. Otero, J.M. Garcia de Otazo, Synth. Met. 159 (2009) 681–688.
[65] T.F. Otero, J.G. Martinez, Adv. Funct. Mater. 23 (2013) 404–416.
[66] T.F. Otero, J.G. Martinez, J. Mater. Chem. B 1 (2013) 26–38.
[67] M. Fuchiwaki, T.F. Otero, J. Mater. Chem. B 2 (2014) 1954–1965.

[68] J.N. Barisci, G.G. Wallace, R.H. Baughman, J. Electroanal. Chem. 488 (2000) 92–98.
[69] J.N. Barisci, G.G. Wallace, R.H. Baughman, J. Electrochem. Soc. 147 (2000) 4580–4583.
[70] J.G. Martinez, T.F. Otero, J. Phys. Chem. B 116 (2012) 9223–9230.
[71] L.V. Conzuelo, J. Arias-Pardilla, J.V. Cauich-Rodríguez, M.A. Smit, T.F. Otero, Sensors 10 (2010) 2638–2674.
[72] T.F. Otero, J. Schumacher, V.H. Pascual, RSC Adv. (2016).
[73] T.F. Otero, H. Grande, J. Rodriguez, Electrochim. Acta 41 (1996) 1863–1869.
[74] M. Fuchiwaki, J.G. Martinez, T.F. Otero, Adv. Funct. Mater. 25 (2015) 1535–1541.
[75] H. Randriamahazaka, Smart Mater. Struct. 20 (2011) 124010.
[76] J.N. Barisci, G.G. Wallace, R.H. Baughman, J. Electrochem. Soc. 147 (2000) 4580–4583.
[77] K. Mukai, K. Asaka, K. Hata, T. Fernández Otero, H. Oike, Chem. Eur. J. 17 (2011) 10965–10971.
[78] P. Giménez, K. Mukai, K. Asaka, K. Hata, H. Oike, T.F. Otero, Electrochim. Acta 60 (2012) 177–183.
[79] J.G. Martínez, T.F. Otero, C. Bosch-Navarro, E. Coronado, C. Martí-Gastaldo, H. Prima-Garcia, Electrochim. Acta 81 (2012) 49–57.
[80] Y. Shao, J. Wang, H. Wu, J. Liu, I.A. Aksay, Y. Lin, Electroanalysis 22 (2010) 1027–1036.
[81] Z. Liu, A.A. Yasseri, J.S. Lindsey, D.F. Bocian, Science 302 (2003) 1543–1545.
[82] M. Łapkowski, M. Zagorska, I. Kulszewicz-Bajer, A. Proń, J. Electroanal. Chem. 341 (1992) 151–163.
[83] A. Abd-Elwahed, R. Holze, Synth. Met. 131 (2002) 61–70.
[84] C. Odin, M. Nechtschein, P. Hapiot, Synth. Met. 47 (1992) 329–350.
[85] K. Aoki, J. Cao, Y. Hoshino, Electrochim. Acta 39 (1994) 2291–2297.
[86] K.-M. Mangold, K. Morgenschweis, K. Jüttner, Electrochim. Acta 44 (1999) 1865–1869.
[87] M.R. Presa, D. Posadas, M.I. Florit, J. Electroanal. Chem. 482 (2000) 117–124.
[88] M. Kalaji, L. Nyholm, L.M. Peter, J. Electroanal. Chem. Interfacial Electrochem. 313 (1991) 271–289.